Acid-Base Synthesis of Aluminum Iodate Hexahydrate Powder as a Promising Propellant Oxidizer

Kelsea K. Miller[a], Shannon E. Creegan[b], Daniel K. Unruh[c], Joseph Pantoya[a,d], Kevin Hill[d], Quan Tran[a], Michelle L. Pantoya[a]

[a] Department of Mechanical Engineering, Texas Tech University, Lubbock, Texas 79409, United States

[b] Purdue Energetics Research Center, Purdue University, West Lafayette, Indiana, 47906 United States

[c] Department of Chemistry and Biochemistry, Texas Tech University, Lubbock, Texas 79409, United State

[d] Combustion Science and Propulsion Research Branch, Naval Air Warfare Center Weapons Division, China Lake, CA 93555, United States

ABSTRACT

An acid-base precipitation reaction is detailed to synthesize pure crystals of the oxidizer rich compound $[Al(H_2O)_6](IO_3)_3(HIO_3)_2$ and described here for the first time. The molecule is called aluminum iodate hexahydrate (AIH) and characterized for its energetic potential as an oxidizer in propellant applications. The synthesis method produced bipyramidal hexagonal crystals that are characterized physically and chemically by microscopy, pycnometry, and X-ray crystallography. Further energetic characterization is performed by bomb calorimetry, and impact, friction, and electrostatic discharge ignition sensitivity. This study introduces the potential of AIH as an alternative solid propellant by comparison to the properties of ammonium perchlorate (AP) and ammonium nitrate (AN).

Key Words Propellant; Oxidizer; Ignition; Iodate; Ammonium Perchlorate; Aluminum

1. Introduction

Advancing solid propellant technologies requires development of new molecular formulations that produce fewer toxic byproducts, maintain thermal stability, show potential performance enhancement, and are safe to handle. Ammonium perchlorate (AP) (NH_4ClO_4) is an example of a common solid oxidizer in propellant formulations used for rocket motors. The exhaust from AP combustion includes 20 wt. % hydrochloric acid and other toxic perchlorates [1].

Ammonium nitrate (AN) (NH_4NO_3) is a propellant oxidizer that eliminates production of chlorinated gases. However, AN is severely hygroscopic and plagued with phase transitions that can occur at room temperature, even before thermal decomposition [1]. New approaches that address the thermal instability of AN may eventually overcome its limited integration into energetic systems [2].

Oxidizers in the periodate family have also been considered for propellant applications but are relatively ignition sensitive, thereby limiting their application in energetic systems. Strategies aimed at desensitizing periodate oxidizers are ongoing, with recent success shown by Kim et al. [3].

An alternative approach to developing high energy solid oxidizers is to consider molecules derived from metal fuels that are common ingredients in propellant formulations. The most prevalent metal fuel in propellant applications is aluminum (Al). Recent literature introduced aluminum iodate hexahydrate iodic acid ($[Al(H_2O)_6](IO_3)_3(HIO_3)_2$) formed on the surface of an aluminum (Al) particle and used to passivate the metal particle [2]–[4]. The iodine-oxygen rich molecule is referred to as aluminum iodate hexahydrate and abbreviated as AIH.

Potential benefits to transforming the nascent aluminum oxide (Al_2O_3) passivation shell into AIH have been documented [4]-[8]. Specifically, low temperature dehydration (~120 °C) coupled with a low energy threshold for dehydration contribute to faster shell decomposition resulting in faster metal oxidation [5]. In fact, the activation energy required for dehydration of the AIH shell surrounding an Al particle is 105.1 kJ/mol and similar to the activation energy for decomposition of AN, AP, and common monomolecular explosives (c.a. ~ 100 kJ/mol) [5]–[7]. Therefore, with a similar activation energy, the AIH passivation shell can produce gaseous oxidizing species at similar time scales as explosives and propellants while also exposing the metal core for rapid oxidation.

While there is still more work required to develop metal passivation shells that stimulate metal reactions, the molecular structure of AIH shown in **Fig. 1** suggests the molecule may have strong oxidizer potential as a pure material. Specifically, in **Fig. 1** the aluminum atom is surrounded by a six-member hydroxyl ring that is further surrounded by iodates. The abundance of hydrogen and oxygen gas available during AIH reaction may provide stimuli for propagating reactions relevant to propellant applications. The synthetic process to form pure crystals of AIH has not previously been reported and AIH is not commercially available.

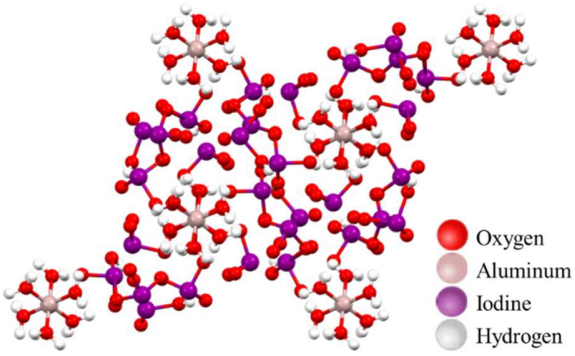

Figure 1. Polyhedral packed molecular structure of AIH generated from the powder diffraction file (PDF) 01-083-1975. The red spheres are oxygen, pink are aluminum, purple are iodine, and white are hydrogen.

On the shell of an aluminum particle, AIH is formed from aqueous solution-based chemical reactions [4]. Using an iodic acid solution, the Al_2O_3 shell surrounding an Al particle is removed (or partially removed). Free H^+ from solution polarize the Al-O bonds in Al_2O_3. But the structure of Al_2O_3 surrounding an Al particle is complex and includes hydration layers capping the surface. In the aqueous solution, a polarization mechanism promotes free Al^{3+} cations to be complexed by water molecules and form $[Al(H_2O)_6]^{3+}$. Therefore, formation of AIH from Al_2O_3 is limited by the concentration of $[Al(H_2O)_6]^{3+}$ in the aqueous solution which is variable depending on the structure of the physisorbed and chemisorbed hydration layers on the Al_2O_3 surface. The wide variability in surface hydration has led to great disparity in AIH concentration that can be formed on the surface of an Al particle. Reports range from 6 to 80% AIH on Al particles [4]-[8].

The objective of this study is to extend synthesis of AIH from a surface passivation shell towards its synthesis in a pure crystalline form as a powder. Based on previous work using Al_2O_3 as the precursor, the hypothesis is that a more hydrated form of alumina such as $Al(OH)_3$ will lead to efficient formation of pure AIH crystals. To accomplish the objective, an acid-base precipitation reaction (APR) is described for the synthesis of pure AIH and the processing variabilities that lead to variations in crystal size are also presented. Based on the high iodine, hydrogen, and oxygen concentrations, another objective is to experimentally measure ignition and reaction metrics for safe handling of this new solid oxidizer.

2. Synthesis and experimental procedures

2.1 Synthesis: pure AIH

The AIH acid-base precipitation reaction (APR) synthesis method is illustrated in **Fig. 2** and can be described in four steps. The overall formation reaction is described by Reactions (R1) and (R2). The enthalpy of formation was estimated by Kalman et al. [8] to be -2831.79 kJ/mol from a summation of the enthalpies of formation for its components (i.e. Al, H_2O, IO_3, HIO_3). Ongoing efforts in molecular dynamic simulations will better determine the theoretical heat of formation.

$$I_2O_5 + H_2O \rightarrow 2HIO_{3\,(aq)} \quad \text{(R1)}$$

$$5HIO_{3\,(aq)} + Al(OH)_3 + 3H_2O \rightarrow Al(H_2O)_6(IO_3)_3(HIO_3)_2 \quad \text{(R2)}$$

In the APR process shown in **Fig. 2**, mechanical mixing is maintained in Steps 1-3 until crystallized AIH particles are removed for filtration in Step 4. The first step begins by dissolving iodine pentoxide (I_2O_5) powder in water at a 1:1 weight ratio. As shown in Reaction (1), this forms an iodic acid solution (HIO_3) with a pH between 1 and 2.

In the second step, aluminum hydroxide $Al(OH)_3$ powder is added to the iodic acid solution (I_2O_5:Al = 10:1) and heated to 90 °C to facilitate dissolution. The solution is mechanically mixed throughout $Al(OH)_3$ dissolution. The solution becomes clear after mixing for approximately 30 minutes indicating that $Al(OH)_3$ dissolved.

In the third step, the solution is removed from heat and a precipitant liquid, acetonitrile (ACN, C_2H_3N), is added at a 1:1 volume ratio. The addition of ACN creates a binary solvent system and allows precipitated AIH crystals to form for collection. Constant mixing conditions are still maintained to promote crystal nucleation.

In the fourth step, AIH crystals are filtered through a Buchner funnel. The crystals are rinsed with a one-to-one mixture of deionized water and the precipitant liquid (i.e., ACN) prior to air drying for approximately four hours or longer, depending on batch size. Purity of the synthesized AIH crystals is confirmed with powder X-ray diffraction (XRD). Collected crystals appear opaque white suggesting AIH is polycrystalline.

For a representative synthesis of AIH with the ratios considered above, 0.018 mol of I_2O_5 in 0.333 mol of H_2O formed the iodic acid. Following dissolution, 7.693 mmol of $Al(OH)_3$ yielded approximately 4.943 mmol of AIH.

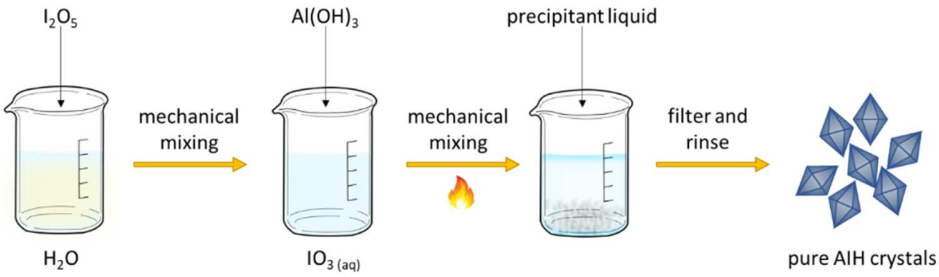

Figure 2. Illustration of APR method for AIH synthesis. *Step 1:* I_2O_5 powder is dissolved in distilled water to form iodic acid solution (IO_3). *Step 2:* $Al(OH)_3$ is mixed to a molar ratio I_2O_5:Al = 10:1. and heated to 90°C until $Al(OH)_3$ is dissolved. *Step 3:* Solution is cooled to room temperature and acetonitrile is added to a volume ratio 1:1. *Step 4:* AIH particles grow and are filtered.

Particle size can be controlled with the duration of time the solvent system in *Step 3* is mechanically mixed. For example, filtering after all observed crystals have separated from the binary system will generate larger crystals (e.g., up to the maximum crystal size of 30 μm, shown in **Fig. 1**) than filtering prior to the complete settling of crystals (e.g., 14 μm). Larger crystal sizes of AIH have also been achieved on the millimeter scale by removing mechanical mixing (or limiting crystal nucleation) and allowing a saturated solution of $Al(OH)_3$ dissolved in iodic acid to slowly evaporate under ambient conditions.

2.2 Experimental methods

2.2.1 Morphology, Particle Size, Density, Equilibrium Reaction Kinetics, and Thermal Stability

Particle size and morphology of the synthesized AIH particles were analyzed from micrographs captured using a Hitachi S-4300VP scanning electron microscope (SEM). Particle sizes were measured using an AccuSizer Syringe Injection Sampler (SIS). The AccuSizer uses the optical particle counting (OPC) method where particles in suspension pass through an illuminated zone which causes light to scatter and create a detected pulse, the magnitude of which is dependent on the particle. Approximately 5 mg of AIH was ultrasonicated with 40 mL of acetone, then loaded into the AccuSizer where the SIS was set to five 30 mL pulls at a flow rate of 20 mL/min.

A Micrometrics AccuPycc 1340 measured AIH density using nitrogen gas displacement pycnometry. The pycnometer was calibrated within the allotted tolerance of 5.155×10^{-4} g/cc. Multiple samples were prepared and tested to determine the repeatability and standard deviation of the measurement. Additionally, varied AIH particle size samples were analyzed. Results show AIH density measurements were independent of particle size and crystallization technique.

Differential scanning calorimetry (DSC) and thermogravimetric (TG) analyses were conducted using a NETZSCH 449 F3 Jupiter simultaneous thermal analyzer (STA). The instrument was calibrated using standard materials (e.g., indium for melting temperature and calcium oxalate for weight loss). Sample size was maintained at 3-5 mg for each run in the STA due to the corrosive nature of halogenated gaseous species. Alumina crucibles contained the powder sample and were lidded with a small pin hole to allow gas escape. All experiments were performed in an argon environment at a heating rate of 10°C/min from 50-600°C. Data were processed using NETZSCH Proteus software. Experiments were performed in triplicate to ensure repeatability.

A thermal stability analysis was performed on AIH by heating the material to 75 °C for 48 hours. The AIH powder was monitored for visual changes such as ignition or color change, and for mass loss. Additionally, XRD measurements on recovered powder post thermal stability analysis were performed. Thermal stability data supplements previous findings on the aging of AIH over a 5-year duration [9].

2.2.2 X-ray Diffraction

The AIH crystals used for reactive testing are an average 30 µm. Larger quality crystals were grown for single crystal X-ray diffraction (SXRD) measurements and are on average 0.9 mm. The XRD patterns were collected on a Rigaku XtaLAB Synergy-*i* Kappa diffractometer equipped with a PhotonJet-*i* X-ray source operated at 50 W (50kV, 1 mA) to generate Mo Kα radiation (λ = 0.71073 Å) and a HyPix-6000HE HPC detector.

After data collection, the unit cell was re-determined using a subset of the full data collection. Intensity data were corrected for Lorentz, polarization, and background effects using the *CrysAlis*^{Pro} [10]. A numerical absorption correction was applied based on a Gaussian integration over a multifaceted crystal and followed by a semi-empirical correction for adsorption applied using the program *SCALE3 ABSPACK* [11]. The software program *SHELXT* [12] was used for the initial structure solution and *SHELXL* [13] was used for refinement of the structure. Both programs were utilized within the OLEX2 software [14]. Hydrogen atoms bound to oxygen atoms were both located in the difference Fourier map and calculated based on I-O bond distances. These positions were then geometrically constrained using the appropriate AFIX commands.

Additional powder XRD data were collected on post burn products recovered from calorimetry testing or post thermal stability analysis. For these XRD measurements, a Rigaku MiniFlex II diffractometer combined with the ICDD PDF 4+ database was used to analyze the residue composition.

Diffraction data were collected from 3-70 ° using Bragg-Brentano geometry while operating in continuous θ-2θ mode. The X-ray source was Cu Kα radiation (λ=1.5418 Å) with a current of 15 mA and a voltage of 30 kV. The powder was mounted in a zero-background holder and diffraction intensities were captured with a D/teX Ultra 1D silicon strip detector.

2.2.3 Calorimetry

Calorimetry was performed to determine the heat of combustion (H_c) of AIH, along with AP and AN for comparison. A Parr 6400 Automatic Isoperibol Bomb Calorimeter (Parr Instrument Company) was used for the experiment with a Parr 1138 Oxygen Combustion Bomb. The delivery pressure for oxygen on the calorimeter was set to 3.1 MPa. Powder samples were suspended in ethylene glycol (EG) that was used as a spiking agent to aid combustion. Multiple experiments were performed and the average H_c and standard deviation are reported, but detailed data are provided in *Supplementary Information*, Table S1.

The H_c was calculated according to instrument calibration parameters that include the energy equivalent of the calorimeter, the observed temperature rise, heat of combustion of the spiking material, mass of the spiking material, and mass of the AIH, AN, or AP powder sample. Corrections for nitric acid, sulfuric acid, and the heating source of the heating wire and cotton thread within the combustion bomb were considered.

2.2.4 Flame Temperature and Specific Impulse (I_{sp}) calculations

Flame temperature and specific impulse are important performance parameters. To supplement the experimental results, CHEETAH [15] calculations were performed for AIH and AP combined with aluminum (Al) fuel and a typical binder used for propellant applications, hydroxyl terminated polybutadiene (HTPB). The calculations used an AIH density of 3.74 g/cm^3 and formation enthalpy of -2831 kJ/mol [8]. Ternary graphs for flame temperature provide insight on the multivariant influence of the reactants. For specific impulse, the optimized reactant mixture was selected for ease of comparison.

2.2.5 Impact & friction ignition sensitivity testing

Impact testing was conducted according to STANAG 4489 [16] and friction testing to STANAG 4487 [17]. The impact tests were performed using an OZM Research Drop Hammer and the friction tests with a BAM Friction Tester. For both impact and friction sensitivity testing, an occurrence of a "No" or negative test is when there is no observable sign of decomposition or reaction such as light, discoloration of material, smoke, or sound. An occurrence of a "Go" or positive test occurs when there is evidence of decomposition or reaction such as light, discoloration of material, smoke, or sound. Impact determination for sensitivity occurred in two instances: (1) if 6-of-6 tests were all negative, then the sensitivity was greater than the value tested, and (2) if 1-of-6 tests were positive, then the sensitivity was equivalent to the value tested. The maximum values were 40 J and 360 N for impact and friction sensitivity, respectively.

2.2.6 Electrostatic Discharge (ESD) ignition sensitivity testing

Electrostatic discharge (ESD) testing was performed using an OZM Research XSpark electrostatic spark sensitivity tester with a XSpark 10 remote control. The accompanying software package for this instrument was the WinSpark 2. The ESD tests were performed according to STANAG 4490 [18] annex A for small scale ESD tests.

Prior to testing, the AIH was stored in a desiccator for one week. The instrument was setup with a gap distance of 1 mm between electrodes and a cylindrical sample container (3.5 x 1 mm). The tests were conducted in fixed mode at a constant capacitance value of 100 nF with varying voltages. A sample was

tested at 1, 1.41, 1.73, 2, 5, and 10 kV. Test energy was calculated from the measured capacitance and voltage [18].

3. Results and discussion

3.1 Materials characterization

A representative image of an AIH crystal is shown in **Fig. 3a**. Crystals have a bipyramidal hexagonal appearance. The particle size distribution for the smallest and largest size ranges synthesized as described in **Fig. 2** are shown in **Fig. 3b and c**.

a.

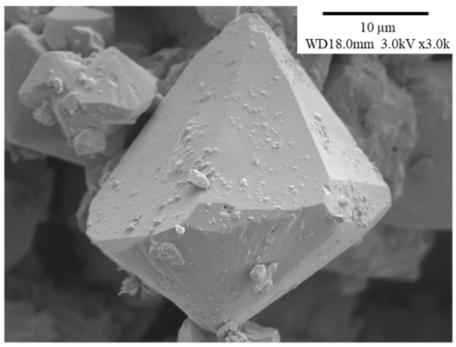

b.

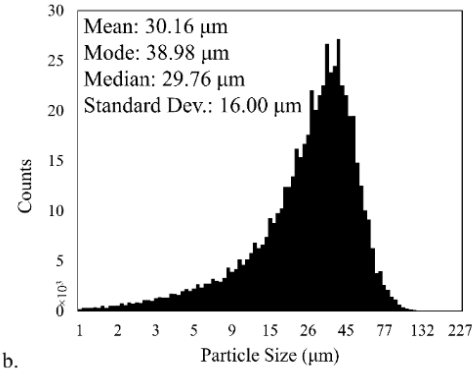

c.

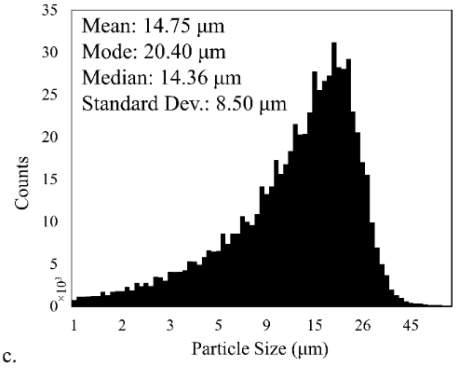

Figure 3. a. SEM image of AIH at an accelerating voltage of 3 kV. b. AIH particle size distribution with mean 30.2 μm obtained from filtering crystals after longer settling times. c. AIH particle size distribution with mean 14.75 μm obtained from filtering crystals after shorter settling times.

The crystallographic data and structure refinement details for AIH are shown in **Table 1**, along with the molecular unit shown in **Fig. 4**. In the Cambridge Crystallographic Data Centre (CCDC) database, there is a reported structure for AIH (CCDC 1597556), but it does not have hydrogen positions listed. An updated model including hydrogen positions for the previously collected data (CCDC 2164952) is reported in *Supplementary Information* Tables S2-S8.

The experimentally measured density (ρ_{meas}) of 3.74 ± 0.02 g/cc is within 2.7% of the density calculated by X-ray crystallography (ρ_{calc} = 3.64 g/cc). The crystal system is hexagonal which is consistent with **Fig. 3a**.

Table 1. Crystallographic data and structure refinement details for AIH.

	AIH
Empirical formula	$AlH_{14}I_5O_{21}$
FW (g/mol)	1011.59
Temperature (K)	100.00(10)
Crystal system	hexagonal
Space group	$P6_3$
a (Å)	16.07320(10)
b (Å)	16.07320(10)
c (Å)	12.36660(10)
α (°)	90
β (°)	90
γ (°)	120
Volume (Å^3)	2766.85(4)
Z	6
ρ_{calc} (g/cm^3)	3.643
μ (mm^{-1})	8.581
F(000)	2760
Crystal size (mm^3)	0.147 × 0.089 × 0.067
Radiation	Mo Kα (λ = 0.71073)
2Θ range for data collection (°)	5.068 to 61.008
Index ranges	$-22 \le h \le 22$, $-22 \le k \le 22$, $-17 \le l \le 17$
Reflections collected	61734
Independent reflections	5629 [R_{int} = 0.0489, R_{sigma} = 0.0206]
Data/restraints/parameters	5629/6/263
Goodness-of-fit on F^2	1.08
Final R indexes [I>=2σ (I)]	R_1 = 0.0171, wR_2 = 0.0403
Final R indexes [all data]	R_1 = 0.0172, wR_2 = 0.0404
Largest diff. peak/hole (e Å^{-3})	1.22/-1.41
Flack parameter	-0.014(12)

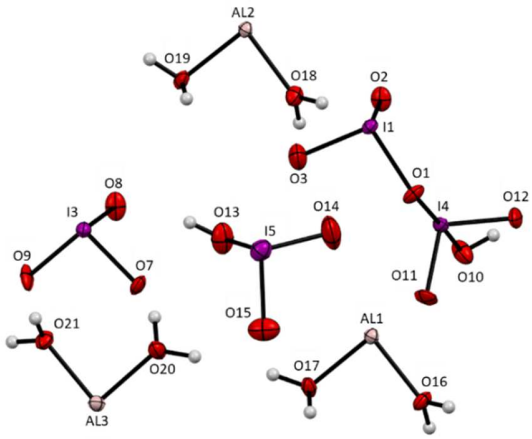

Figure 4. Asymmetric unit of AIH with ellipsoids drawn at the 50% probability level.

Piezoelectricity has been shown to facilitate ignition of energetic materials through electromechanical sensitization [19]-[22]. Crystal symmetry governs the categorization of piezoelectric materials and the piezoelectric effect is only observed in crystalline materials that are non-centrosymmetric [19]. The space group $P6_3$ (**Table 1**) is a non-centrosymmetric crystal structure such that AIH has piezoelectric properties similar to the octahydrate iodate crystals investigated in Kidyarov [20]. For reference, the space groups of the readily occurring polymorphs of AP and AN under ambient conditions are orthorhombic Pnma (centrosymmetric) [21], [22] and orthoromic Pmmn (centrosymmetric) [23], respectively (i.e., AP and AN are not piezoelectric materials). Further characterization is needed to measure piezoelectric effects in AIH for energetic material applications, but the lattice structure reported in **Table 1** indicates AIH has piezoelectric properties.

Figure 5 shows the powder XRD pattern for AIH powder. Thermal stability analysis on AIH showed no signs of discoloration or ignition and no measurable change in mass. The XRD analysis of recovered material showed no change in crystallinity following the analysis (**Fig. 5**). All results indicate AIH is thermally stable.

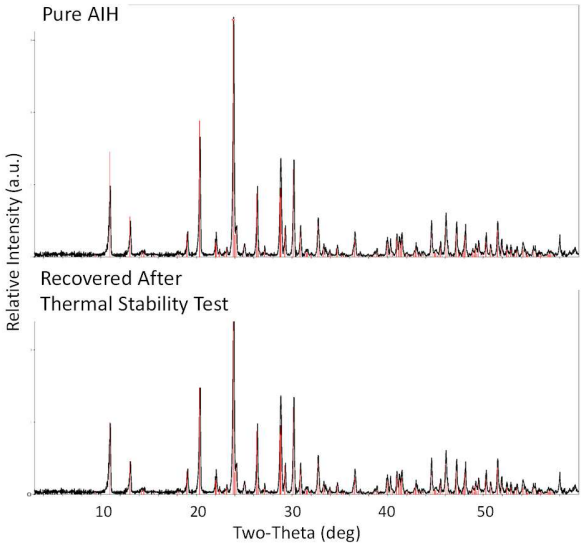

Figure 5. Diffraction pattern of pure AIH (top) and AIH recovered post-thermal stability analysis (bottom) (PDF 04-009-2066).

Table 2 summarizes the properties of AIH in comparison to AN and AP. The oxygen balance (OB) for AIH is calculated in Eq. (1) and global decomposition is shown in Reaction (R3).

$$OB = \frac{-1600}{MW}(2n_C + 0.5n_H - n_O + n_{mo}) \quad (1)$$

$$Al(H_2O)_6(IO_3)_3(HIO_3)_2 \rightarrow \frac{1}{2}Al_2O_{3\,(s)} + 7H_2O_{(v)} + \frac{5}{2}I_{2\,(v)} + 6.25O_{2\,(v)} \quad (R3)$$

In Eq. (1), *MW* is the molecular weight of AIH (1011, **Table 2**), *n* is the number of moles of carbon (0), hydrogen (14), and oxygen (21) in the empirical formula of AIH, and n_{mo} is the number of moles of oxygen in the metallic oxide produced (1.5). The *OB* is reported in terms of 100 g and for AIH, OB is +20. **Table 2** also shows the markedly higher density of AIH compared with AN and AP.

Table 2. Comparison of physical and chemical properties of AIH compared to previously reported values for AP and AN. Safety metrics including impact (IS), friction (FS), and electrostatic sensitivities (ES) are also tabulated.

	AIH	*AN [1]*	*AP [1]*
Formula	$[Al(H_2O)_6](IO_3)_3(HIO_3)_2$	NH_4NO_3	NH_4ClO_4
FW (g/mol)	1011.59	80.04	117.49
Ω (%)	+20	+ 20	+ 27
ρ_{meas} *(g/cm³)*	3.74	1.72	1.95
T_{dec} *(°C)*	195*	210	320
H_c *(kJ/g)*	1.63	2.08(1.45)**	3.04(1.42-2.71)**
IS (J)	> 40	> 40	15
FS (N)	> 128	> 360	> 320
ES (J)	> 5	> 1.5	> 5

*Note that AIH dehydration onset is 120°C, followed by decomposition at 195°C
**Measured values are reported, literature [1] values are in parenthesis.

Figure 6 shows the DSC (green curve) and TGA (black curve) for AIH. The onset of AIH dehydration is 120°C corresponding to the first endothermic peak and first stage of mass loss. Following dehydration, molecular decomposition onset is 195°C, as indicated in **Table 2**. It is useful to note that even upon dehydration, AIH continues to show endothermic decomposition suggesting its stability for safe transport. Gas generation from the TGA analysis also indicates nearly 95% of AIH products are gas phase species (see R3).

Overall, the equilibrium decomposition process for AIH includes four stages of endothermic and mass loss activity. The gas phase products produced are iodine, oxygen, and water vapor. In a high temperature reactive environment, water vapor will further produce hydrogen gas. The molecular formula of AIH compared to AP and AN (**Table 2**) shows that AIH will produce more hydrogen than AN or AP. Formation of hydrogen gas can be used as a fuel source in some energetic applications. Moreover, the iodine gas generated can be used to neutralize spore forming bacteria, such as anthrax, thereby sterilizing biologically contaminated environments.

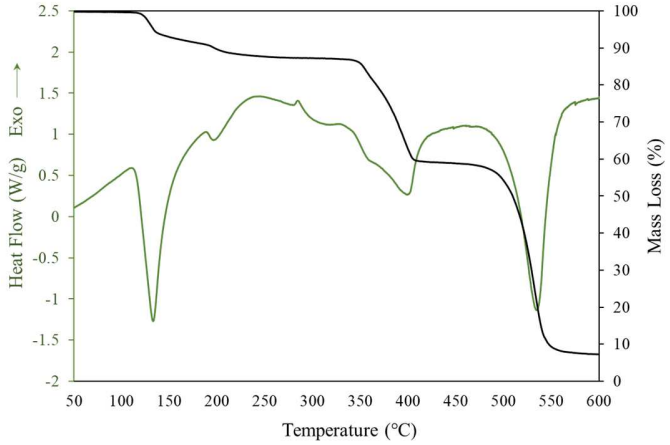

Figure 6. Thermal equilibrium data collected at 10 °C/min heating rate in an argon environment. The DSC heat flow (left axis and data in green) and TG mass loss (right axis and data in black) are shown as a function of temperature.

The measured H_c for AIH is exothermic and 1.63 ± 0.72 kJ/g. Note that H_c for AP reported previously [1] (and shown in parenthesis in **Table 2**) varies from measured values here. The measured value for AP is 3.04 $\pm$ 0.31 kJ/g. Wide variations for AP are not surprising because the decomposition mechanism for AP is complex and can vary widely based on multiple factors such as particle size, surface features, and conditions of the measurement. Combining AP with EG spiking agent has been shown to modify the AP crystal habit and increase H_c, consistent with the measurements shown here [24]. Also, H_c for AN is 2.08 $\pm$ 0.24 kJ/g, and slightly higher than the previously reported value (**Table 2**). Both average measured values for AP and AN are higher than for AIH but with standard deviations considered, AN and AIH are comparable while AP is highest, on a per mass basis. However, with the increased density of AIH relative to AN and AP (**Table 2**), the same volume of oxidizer will lead to an overall increase in AIH energy release upon combustion.

Figure 7 shows predicted results for flame temperature and specific impulse for AIH and AP combined with a representative fuel, Al, and a propellant binder, HTPB. The ternary graphs provide perspective on three variables within the propellant formulation simultaneously and indicate similar optimized stoichiometries for the ternary systems. The specific impulse (Isp) data are all optimized by

sweeping the fuel mass. The Isp data assume a 100:1 area ratio of the nozzle, into a vacuum, and a chamber pressure of 2.0 MPa (300 psi), which is standard for comparison. While Isp is generally lower for AIH, the density specific impulse is higher owing to the higher density of AIH.

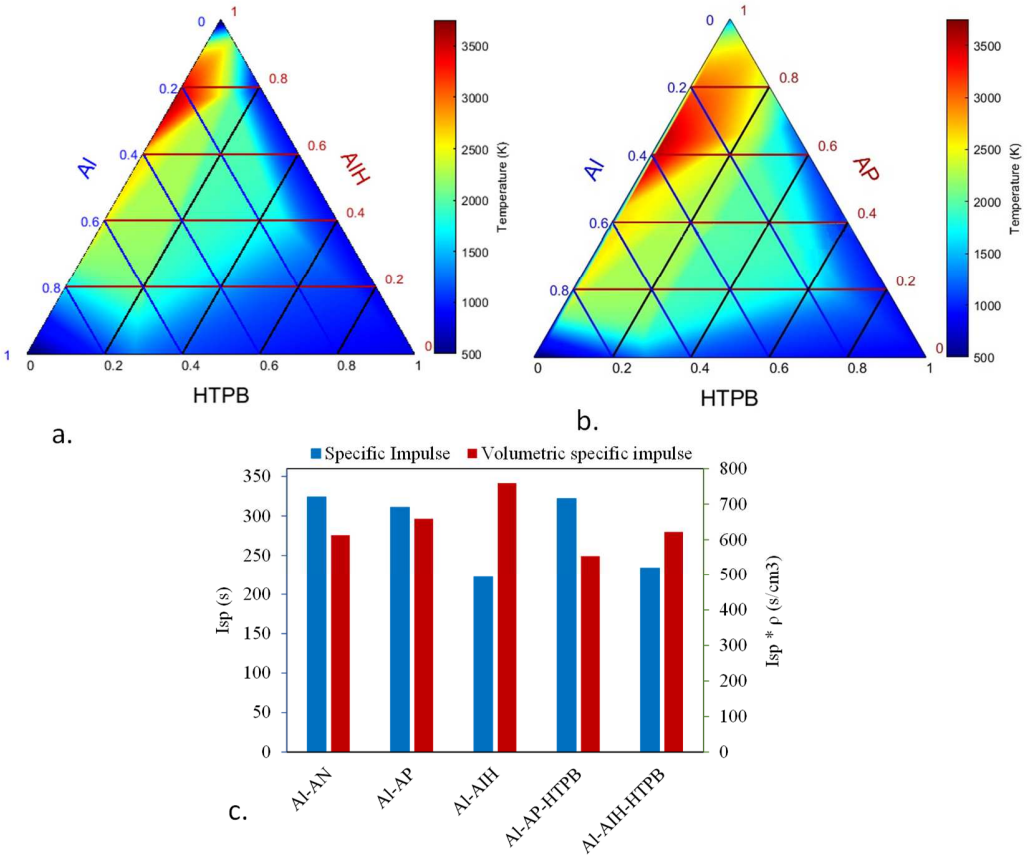

Figure 7. Flame temperature calculations for the ternary mixtures of AIH or AP combined with Al and HTPB (a-b). Specific impulse (blue) and volumetric specific impulse (red) calculations for mixtures including AIH, AP, Al, HTPB. Note calculations performed for weight percent concentrations.

For qualitative comparison, preliminary burn tests are visually shown in **Fig. 8** for AIH combined with Al powder compared with AP combined with Al powder. In both cases, 80 nm Al powder was used and mixtures were spatula mixed as dry powders with weight percentages of 80% oxidizing species and 20% Al fuel powder. The mixtures are contained in a ceramic crucible typically used to hold powders in the DSC-TGA instrument (i.e., ~20 mg of powder mixture in a 10 mm diameter, 25 mm height ceramic crucible). Powders were ignited with a 40W CO_2 laser, and a Phantom 2640 high speed camera recorded the reaction. Overall, AIH +Al produced a voluminous flame that has a large, bright plume. In contract, AP + Al produced a stringy plume with solid particle ejections that appear to result from agglomeration of particles. Also, AIH+Al appeared to ignite more easily than AP+Al, but these observations are qualitative and may be associated with oxidizer particle size influences. For example, the AP powder was average 50 µm nominal size while the AIH is average 30 µm nominal size.

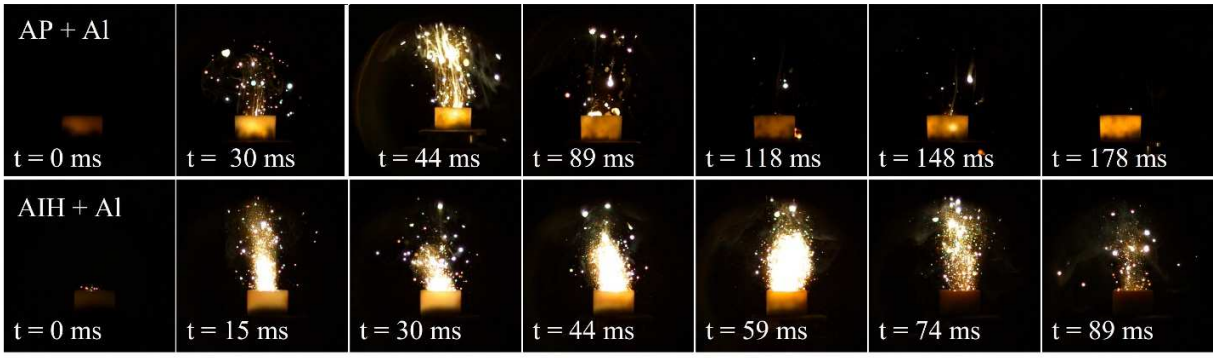

Figure 8. Sequence of still frame images qualitatively illustrating powder burns from mixtures of mass ratio 80:20 AP:Al (top) and AIH:Al (bottom). Note powder mixtures are contained in a ceramic crucible.

The post-burn solid products recovered from calorimetry testing were alpha- and eta-aluminum oxide (α- and η-Al_2O_3) as indicated in **Figure 9**. The weight concentrations from whole pattern fitting using Rietveld Refinement analysis within the MDI Jade V9.1.1 software was 64% α-Al_2O_3 and 36% η-Al_2O_3. The presence of these specific crystalline phases suggests: (1) AIH completely decomposed upon reaction based on the decomposition mechanism reported by Shancita et al. [25], and (2) reaction temperatures reached at least 600-800 °C [26] to produce the stable and metastable phases of alumina.

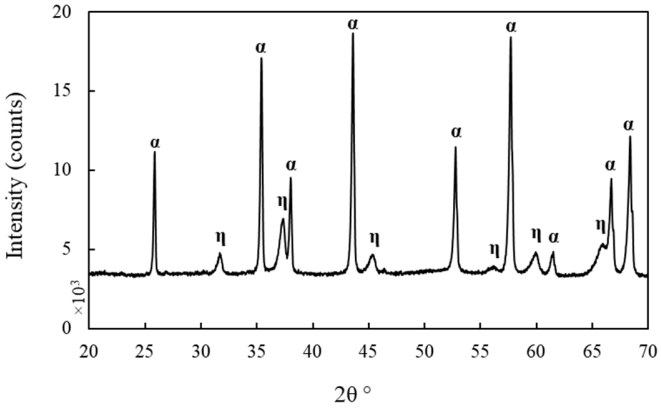

Figure 9. Diffraction pattern of post burn products recovered from Parr bomb calorimetry testing. Two crystalline phases are labelled, α- and η-Al_2O_3 (PDF 04-004-2852 and 04-007-2867, respectively).

No sign of decomposition or reaction of AIH was detected during impact testing. After the initial impact value (10 J) yielded a "No", the impact value was increased by 10 J intervals until the max value of 40 J was reached. A total of six runs at 40 J all yielded "No". Therefore, the AIH powder was determined to be insensitive to impact with an impact sensitivity greater than 40 J as indicated in **Table 2**.

Regarding friction testing, a test was determined to be a "Go" when the white appearance of AIH was altered to a light brown indicating AIH decomposition. In the instance of two occurrences indicating a positive result, the amount of force applied is decreased by 120 J. There are two observed "Go" tests for 360 N and 240 N each. Two consecutive "No" results are achieved for 120 N so the weight position on the arm of the BAM friction tester increased. Five negative results are observed for 128 N, and one positive test occurred. Therefore, AIH powder was determined to be sensitive to friction with a sensitivity

value of 128 N. According to standardized friction testing [17], if one of six tests is a "Go" then the friction sensitivity is equivalent to the value tested.

There was no observed indication of decomposition or reaction of AIH from ESD tests at 1, 1.41, 1.73, 2, 5, and 10 kV. Powder AIH samples were further tested at 10 kV in six separate trials. All trials showed no sign of decomposition or reaction. Therefore, the ESD ignition sensitivity for AIH is greater than 5 J as indicated in **Table 2**.

4. Concluding Remarks

Aluminum iodate hexahydrate (AIH) iodic acid was synthesized by an acid-base precipitation reaction using aluminum hydroxide ($Al(OH)_3$) and aqueous iodic acid as the precursory materials. Detailed synthesis procedures are reported herein. Varied particle sizes were produced and characterized for their energetic properties. Crystals of AIH are opaque white indicating polycrystallinity and its molecular structure indicates piezoelectric property features. The molecule of AIH has an oxygen balance of +20, density nearly three times larger than AN and AP, and comparable safety metrics. While the heat of combustion of AIH is exothermic and comparable to AN and AP, the thermal equilibrium decomposition of AIH is entirely endothermic with nearly 95% gas generation capability.

The AIH decomposition products are iodine and oxygen gas and water vapor, less toxic than nitrate-based gases or hydrochloric acid. Also, upon water vapor decomposition, AIH becomes an excellent hydrogen gas generator, with more hydrogen gas available than AN or AP can offer. Moreover, the iodine gas can be used to neutralize bacteria, thereby sterilizing biologically contaminated environments. Potential chemical benefits of AIH must be balanced by performance demands but the clean oxidizers, hydrogen gas availability, and iodine gas generation all offer potential for AIH to supplement or even replace other oxidizers, depending on the application. Further characterization studies of AIH as a propellant oxidizer are on-going.

Author contributions

K. Miller managed and led experimental activities. K. Miller and M. Pantoya contributed equally to the writing of this manuscript. M. Pantoya supervised this research. S. Creegan performed ignition sensitivity testing (friction, ESD, and impact). D. Unruh performed XRD measurements reported in Table 1. Q. Tran performed heat of combustion experimentation for ammonium nitrate and ammonium perchlorate. J. Pantoya and K. Hill performed flame temperature and specific impulse calculations.

Data Availability

The data that supports the findings of this study are available from the corresponding author upon reasonable request.

Declaration of Competing Interest

The authors declare that they have no known competing financial interests or personal relationships that could have appeared to influence the work reported in this paper.

Funding sources and acknowledgments

The authors are thankful for support from the US Army Research Office grant number W911NF-11-1-0439 as well as the Office of Naval Research (ONR) STEM grant number N00014-21-1-2519 and DOE STEM grant DE-NA0003988.

Dr. Davin Piercey is gratefully acknowledged for assistance with ignition sensitivity testing. We are also grateful for assistance from Mr. Clayton Miller and Mr. Quan Tran at Texas Tech University for their assistance with synthesis and calorimetry experiments.

References

[1] T. M. Klapötke, *Chemistry of High-Energy Materials*. De Gruyter, 2017.

[2] D. K. Smith, D. K. Unruh, and M. L. Pantoya, "Replacing the Al2O3 Shell on Al Particles with an Oxidizing Salt, Aluminum Iodate Hexahydrate. Part II: Synthesis," *J. Phys. Chem. C*, vol. 121, no. 41, pp. 23192–23199, Oct. 2017.

[3] D. K. Smith, M. N. Bello, D. K. Unruh, and M. L. Pantoya, "Synthesis and reactive characterization of aluminum iodate hexahydrate crystals [Al(H2O)6](IO3)3(HIO3)2," *Combust. Flame*, vol. 179, pp. 154–156, May 2017.

[4] J. L. Gottfried, D. K. Smith, C.-C. Wu, and M. L. Pantoya, "Improving the Explosive Performance of Aluminum Nanoparticles with Aluminum Iodate Hexahydrate (AIH)," *Sci. Rep.*, vol. 8, no. 1, p. 8036, 2018.

[5] S. K. Bhattacharia, K. K. Miller, J. L. Gottfried, and M. L. Pantoya, "Strategy for Enhancing Fast Energy Release from Aluminum Nanoparticles Based on Activation Energy Analysis," *J. DoD Res. Eng.*, 2022.

[6] R. Gunawan and D. Zhang, "Thermal stability and kinetics of decomposition of ammonium nitrate in the presence of pyrite," *J. Hazard. Mater.*, vol. 165, no. 1–3, pp. 751–758, Jun. 2009.

[7] S. Vyazovkin and C. A. Wight, "Kinetics of Thermal Decomposition of Cubic Ammonium Perchlorate," *Chem. Mater.*, vol. 11, no. 11, pp. 3386–3393, Nov. 1999.

[8] J. Kalman, D. K. Smith, K. K. Miller, S. K. Bhattacharia, K. R. Bratton, and M. L. Pantoya, "A strategy for increasing the energy release rate of aluminum by replacing the alumina passivation shell with aluminum iodate hexahydrate (AIH)," *Combust. Flame*, vol. 205, pp. 327–335, Jul. 2019.

[9] Pesce-Rodriguez, R.A., Gottfried, J.L., Giri, L, Miller, K.K., Pantoya, M.L., High-Pressure Thermal and Aging Behavior of Aluminum Iodate Hexahydrate, DEVCOM Army Research Laboratory (USA), Report No. ARL-TN-1072, Aberdeen, MD, USA, August 2021.

[10] CrysAlisPRO, Oxford Diffraction / Agilent Technologies US Ltd, Yarnton, England, 2018.

[11] Gorbitz, C.H., Scaling/Illuminated Volume Correction, *Acta Cryst.* vol. B55, pp. 1090-1098, 1999.

[12] G. M. Sheldrick, "Crystal structure refinement with SHELXL," *Acta Crystallogr. C*, vol. 71, no. 1, pp. 3–8, Jan. 2015.

[13] G. M. Sheldrick, "SHELXT - Integrated space-group and crystal-structure determination," *Acta Crystallogr. Sect. A*, vol. A71, no. 1, pp. 3–8, Jan. 2015.

[14] O. V Dolomanov, L. J. Bourhis, R. J. Gildea, J. A. K. Howard, and H. Puschmann, "OLEX2: a complete structure solution, refinement and analysis program," *J. Appl. Crystallogr.*, vol. 42, no. 2, pp. 339–341, Apr. 2009.

[15] Fried, L., Souers, P., CHEETAH: A Next Generation Thermochemical Code, Lawrence Livermore National Laboratory Technical Report UCRL-ID-117240, Livermore, CA, USA, Nov. 1994.

[16] *NATO Standardization Agreement (STANAG) on Explosives, Impact Sensitivity Test*, vol. no. 4489,

no. 1. Brussels: United Nations Economic Commission for Europe, 2002.

[17] *NATO Standardization Agreement (STANAG) on Explosives, Friction Sensitivity Tests*, vol. no. 4487, no. 1. Brussels, 2002.

[18] *NATO standardization agreement (STANAG) on explosives, electrostatic discharge sensitivity test(s)*, vol. no. 4490, no. 1. Brussels, 2002.

[19] K. Uchino, *Advanced Piezoelectric Materials*. Woodhead Publishing, 2010.

[20] B. I. Kidyarov, "Growth of polar Al(IO3)3 · 8H2O crystals from aqueous solutions," *Bull. Russ. Acad. Sci. Phys.*, vol. 74, no. 9, pp. 1255–1256, 2010.

[21] N. Yedukondalu and G. Vaitheeswaran, "Polymorphism, Phase Transition, and Lattice Dynamics of Energetic Oxidizer Ammonium Perchlorate under High Pressure," *J. Phys. Chem. C*, vol. 123, no. 4, pp. 2114–2126, Jan. 2019.

[22] G. Peyronel and A. Pignedoli, "A three-dimensional X-ray redetermination of the crystal structure of ammonium perchlorate," *Acta Crystallogr. Sect. B*, vol. 31, no. 8, pp. 2052–2056, Aug. 1975.

[23] R. S. Chellappa, D. M. Dattelbaum, N. Velisavljevic, and S. Sheffield, "The phase diagram of ammonium nitrate," *J. Chem. Phys.*, vol. 137, no. 6, p. 64504, Aug. 2012.

[24] Kohga, M., Tsuzuki, H., Burning-Rate Characteristics of Composite Propellant Using Ammonium Perchlorate Modified by Ethylene Glycol, *Journal of Propulsion and Power*, vol. 27, no. 3, pp. 1-6, Aug. 2009

[25] I. Shancita, K. K. Miller, P. D. Silverstein, J. Kalman, and M. L. Pantoya, "Synthesis of metal iodates from an energetic salt," *RSC Adv.*, vol. 10, no. 24, pp. 14403–14409, 2020.

[26] I. Levin and D. Brandon, "Metastable Alumina Polymorphs: Crystal Structures and Transition Sequences," *J. Am. Ceram. Soc.*, vol. 81, no. 8, pp. 1995–2012, Aug. 1998.

Table of Contents Graphic